Available online at www.sciencedirect.com
SCIENCE DIRECT®
Journal of Solid State Chemistry 178 (2005) 339–345
JOURNAL OF SOLID STATE CHEMISTRY
www.elsevier.com/locate/jssc

Synthesis, phase relationship and crystal structure of the new binary compound $Ir_{13}Al_{45}$

Magnus Boström*, Rainer Niewa, Yurii Prots, Yuri Grin

Max-Planck-Institut für Chemische Physik fester Stoffe, Nöthnitzer Strasse 40, 01187 Dresden, Germany

Received 4 August 2004; received in revised form 21 October 2004; accepted 29 October 2004

Abstract

The new phase $Ir_{13}Al_{45}$ was synthesized in equilibrium with an aluminum-rich melt. Its crystal structure was established from single-crystal diffraction data. The compound crystallizes in the space group *Pnma* and represents a novel structure type (Pearson symbol *oP*232, $a = 16.760(2)$ Å, $b = 12.321(1)$ Å, $c = 17.425(2)$ Å). The structure can essentially be described as a simple hexagonal column packing of pseudopentagonal columns formed by irregular Al polyhedra centered by Ir atoms. $Ir_{13}Al_{45}$ forms peritectically at 895 °C and exists in equilibrium with the melt in a narrow temperature interval of 19 °C.

Keywords: Intermetallic compounds; Ir–Al binary system; Crystal structure; X-ray diffraction; Phase equilibria

1. Introduction

The Ir–Al system is known to contain the intermediate phases Ir_2Al_9 (Co_2Al_9 type, *mP*22) [1,2], $IrAl_3$ ($NaAs_3$ type, *hP*8) [3,4], $IrAl_{2.75}$ (own type, *cP*60) [4–6] and IrAl (CsCl type, *cP*2) [4,7–8]. Ferro et al. [4] reported the existence of the phase $IrAl_{3.75}$ (78 at% Al) without giving any structural information, and later Axler et al. [9] reported a phase with the composition Ir_4Al_{13} (76.5 at% Al) found during an investigation of the Ir–Al phase diagram. None of the two groups mentioned the phase reported by the other. In addition, a metastable decagonal quasicrystalline phase has been identified by electron diffraction in the aluminum-rich part of the Ir–Al system [10,11]. Besides showing interesting structures, Ir–Al alloys have potential use as refractory superalloys, e.g., for use in heat and oxidation-resistant coatings [12–14]. Future applications require a more detailed knowledge about conditions of formation and the structures of the binary phases.

During syntheses of Ir_2Al_9 [2], we obtained single crystals with unit cell parameters hitherto unobserved in the Ir–Al system. In this work, we present the crystal structure solution and refinement of the new compound $Ir_{13}Al_{45}$, as well as its phase relations.

2. Experimental

Single crystals of $Ir_{13}Al_{45}$ were prepared in a aluminum-rich self flux from 0.063 g Ir (sheet, 99.9%, Lamprecht) and 0.667 g Al (granules, 99.99%, Chempur). The elements (nominal composition $Ir_{1.3}Al_{98.7}$) were weld-sealed in a tantalum container fitted with a tantalum filter, which had been manufactured from tantalum plate with five 0.5 mm wide holes. The container was subsequently sealed inside an evacuated quartz tube. The mixture was heated to 900 °C at a rate of 450 °C/h. Thereafter, the temperature was decreased by 2 °C/h to 680 °C where the melt was removed by high-temperature centrifugation aided filtration [15]. Block-shaped single crystals with well-exhibited faces were isolated and a part of one of them was used for the single-crystal X-ray diffraction experiment. A single-

*Corresponding author.
E-mail address: bostroem@cpfs.mpg.de (M. Boström).

0022-4596/$ - see front matter © 2004 Elsevier Inc. All rights reserved.
doi:10.1016/j.jssc.2004.10.037

phase bulk sample for unit cell refinement was prepared from 0.269 g Ir and 0.270 g Al (nominal composition $Ir_{12.3}Al_{87.7}$) in the same way as described above, except from the sample this time was heated at a constant temperature of 890 °C for 41 h before the removal of the melt. A two-phase sample containing $Ir_{13}Al_{45}$ and Ir_2Al_9 for differential thermal analysis (DTA) was prepared analogously (0.217 g Ir and 0.219 g Al, nominal composition $Ir_{12.2}Al_{87.8}$), but heated at 877 °C for 48 h before the removal of the melt. This temperature is just above the peritectic temperature of the more Al-rich neighboring phase Ir_2Al_9. During the centrifugation a small decrease in temperature must be assumed, which allows the formation of a small amount of the latter phase, resulting in a two-phase sample. The two-phase samples for investigation of the homogeneity range were prepared by sintering of the fine milled and pressed mixture of single crystals of $Ir_{13}Al_{45}$ with the neighboring phases Ir_2Al_9 or 'Ir_4Al_{13}' at 800 °C for 120 h.

Single-crystal X-ray diffraction data were collected on a Rigaku Mercury CCD diffraction system using Mo$K\alpha$ radiation ($\lambda = 0.71069$ Å). The measured intensities were corrected for absorption using multi-scans in the Laue class *mmm*. Systematic extinctions ($0\,k\,l$ with $k + l \neq 2n$ and $h\,k\,0$ with $h \neq 2n$) in the measured reflection set indicated the possible space groups $Pna2_1$ (no. 33) and *Pnma* (no. 62). The crystal structure was successfully solved in the space group *Pnma* by direct methods using the SHELXS97 program [16] and was then refined with the JANA2000 program [17]. The refined parameters were a scale factor, atomic coordinates, anisotropic displacement parameters and an extinction coefficient. Relevant parameters for the data collection and refinement are summarized in Table 1. The final atomic coordinates and displacement parameters are given in Tables 2 and 3.

The compositions of several single crystals were analyzed with a Philips XL30 scanning electron microscope equipped with an EDAX Phoenix EDX detector (Röntgenanalytik Messtechnik GmbH). Special care was taken to identify possible foreign elements in the EDX spectra.

X-ray powder diffraction patterns with LaB_6 ($a = 4.15692(1)$ Å) added to the samples as internal standard were collected with a Huber Imaging Plate Guinier Camera G670 using Cr$K\alpha_1$ ($\lambda = 2.2896$ Å) radiation. The unit cell parameters were refined from powder data with the CELREF [18] program. These values were subsequently used for the calculation of the interatomic distances.

DTA was carried out (DSC 404, Netzsch, thermocouple type S, heating/cooling rate 10 K/min) in argon atmosphere (Messer–Griesheim, 99.999%, additionally purified by passing over BTS-catalyst, Merck) using Al_2O_3 pans. The melting points of five pure metals were employed for temperature calibration.

Table 1
Crystallographic information and data handling for $Ir_{13}Al_{45}$[a]

Crystal data	
Chemical formula	$Ir_{13}Al_{45}$
Crystal system	Orthorhombic
Space group	*Pnma* (no. 62)
Z	4
a (Å)[b]	16.760(2)
b (Å)[b]	12.321(1)
c (Å)[b]	17.425(2)
V (Å^3)[b]	3598.3(6)
Density calc. (g/cm^3)	6.85
Crystal form	Irregular
Crystal size (mm^3)	$0.030 \times 0.040 \times 0.055$
Color	Gray metallic
Absorption coefficient (mm^{-1})	49.0
Data collection	
Diffraction system	Rigaku AFC7 Mercury CCD
Radiation, λ (Å)	Mo$K\alpha$, 0.71069
No. of measured reflections	29922
Range of $h\,k\,l$	$-24 \leqslant h \leqslant 23$ $-18 \leqslant k \leqslant 18$ $-18 \leqslant l \leqslant 25$
Absorption correction	Multi-scan
T_{max}/T_{min}	2.42
R_{int}	0.034
Refinement	
Refinement on	F
No. of independent reflections	5627
No. of independent observed reflections	5020
Observation criterion	$I > 3\sigma(I)$
No. of reflections used in refinement	5627
No. of parameters refined	290
Weighting scheme	Unit
$R(F)_{all}$, w$R(F)_{all}$, $R(F)_{obs}$	0.035, 0.034, 0.029
GOF_{all}	0.97
$\Delta\rho_{max}$, $\Delta\rho_{min}$, (e/Å^3)	0.9, −2.4
Extinction model	Gaussian isotropic [27]
Extinction coefficient	0.0611(8)

[a]Further details of the crystal structure investigation can be obtained from Fachinformationszentrum Karlsruhe, 76344 Eggenstein-Leopoldshafen, Germany (Fax: (49) 7247-808-666; e-mail: crysdata@fiz.karlsruhe.de) on quoting the depository number CSD391249.

[b]The standardized lattice parameters from powder diffraction data are listed. The lattice parameters from the single-crystal data agree with the listed values within two e.s.d's.

3. Results and discussion

The crystal structure determination revealed a predominantly ordered structure with 38 crystallographically independent atomic positions. Irregularities in the atomic displacement were found for the positions Al19 and Al25. In the case of Al19, the ratio $U_{22} \gg U_{11} \approx U_{33}$ suggested a shift of this atom from the mirror plane. The difference electron density in the vicinity of the Al19 position had a non-spherical distribution (elongation along [010], Fig. 1, top). The deviation is small but

Table 2
Final atomic coordinates and isotropic displacement parameters (in Å^2) for $Ir_{13}Al_{45}$

Atom	Site	x	y	z	U_{eq}/U_{iso} [a]
Ir1	8*d*	0.06315(2)	0.08448(3)	0.41271(2)	0.00468(8)
Ir2	8*d*	0.07052(2)	0.55900(3)	0.17646(2)	0.00491(8)
Ir3	8*d*	0.29985(2)	0.06972(3)	0.07315(2)	0.00452(8)
Ir4	8*d*	0.30294(2)	0.56570(3)	0.33485(2)	0.00468(8)
Ir5	4*c*	0.06335(3)	1/4	0.01872(3)	0.0057(1)
Ir6	4*c*	0.07652(3)	1/4	0.64326(3)	0.0054(1)
Ir7	4*c*	0.17775(3)	1/4	0.24935(3)	0.0044(1)
Ir8	4*c*	0.29272(3)	1/4	0.49806(3)	0.0049(1)
Ir9	4*c*	0.41754(3)	1/4	0.26196(3)	0.0046(1)
Al1	8*d*	0.0057(2)	0.5725(2)	0.3222(2)	0.0080(7)
Al2	8*d*	0.0346(2)	0.0556(3)	0.0564(2)	0.0093(7)
Al3	8*d*	0.1261(2)	0.0636(3)	0.2842(2)	0.0115(8)
Al4	8*d*	0.1547(2)	0.1244(3)	0.5318(2)	0.0099(7)
Al5	8*d*	0.1710(2)	0.1119(3)	0.1429(2)	0.0138(8)
Al6	8*d*	0.1856(2)	0.5337(3)	0.4189(2)	0.0145(8)
Al7	8*d*	0.1895(2)	0.6361(3)	0.2442(2)	0.0090(7)
Al8	8*d*	0.1897(2)	0.5800(3)	0.0852(2)	0.0095(7)
Al9	8*d*	0.2925(2)	0.1320(3)	0.2938(2)	0.0158(9)
Al10	8*d*	0.3126(2)	0.6380(2)	0.4855(2)	0.0075(7)
Al11	8*d*	0.3402(2)	0.5640(2)	0.1873(2)	0.0070(7)
Al12	8*d*	0.3472(2)	0.0676(3)	0.4372(2)	0.0127(8)
Al13	8*d*	0.4239(2)	0.1121(2)	0.1536(2)	0.0056(7)
Al14	8*d*	0.4382(2)	0.0684(3)	0.0072(2)	0.0081(7)
Al15	8*d*	0.4418(2)	0.0472(2)	0.3000(2)	0.0080(7)
Al16	8*d*	0.5581(2)	0.1329(3)	0.6085(2)	0.0091(7)
Al17	4*c*	0.0296(3)	1/4	0.4933(2)	0.007(1)
Al18	4*c*	0.0423(3)	1/4	0.3243(2)	0.007(1)
Al19[b]	8*d*	0.0498(3)	0.2365(6)	0.1688(3)	0.008(1)
Al20	4*c*	0.1352(3)	1/4	0.7789(2)	0.009(1)
Al21	4*c*	0.1807(3)	1/4	0.4002(2)	0.009(1)
Al22	4*c*	0.2293(3)	1/4	0.6356(3)	0.008(1)
Al23	4*c*	0.2660(3)	1/4	0.8680(2)	0.0054(9)
Al24	4*c*	0.2984(3)	1/4	0.1580(2)	0.007(1)
Al25[c]	4*c*	0.3337(2)	1/4	0.0102(2)	0.0035(6)
Al26	4*c*	0.4222(3)	1/4	0.4118(3)	0.009(1)
Al27	4*c*	0.4243(3)	1/4	0.5731(3)	0.017(1)
Al28	4*c*	0.4263(2)	1/4	0.8902(2)	0.0049(9)
Al29	4*c*	0.4721(3)	1/4	0.7260(2)	0.008(1)

[a] $U_{eq} = \frac{1}{3}\sum_i\sum_j U_{ij}a_i^*a_j^*a_ia_j$.
[b] Occupancy 0.5. Refined with isotropic displacement parameter.
[c] Refined with isotropic displacement parameter.

recognizable. This position was successfully described as split in the final refinement. The atom Al25 had the negative value of $U_{22} = 0.001(2)$Å. However, inspection of the difference Fourier maps in the vicinity of this position showed in both the (010) and (001) planes only a very minute deviation from a spherical distribution of the electron density (Fig 1, bottom). The deviation is smaller compared with the Al19 position. Nevertheless, the anisotropic refinement failed and this position was finally refined isotropically. Also, the Al28 position presents similar behavior. The U_{eq} value is lower compared with the values for the other Al atoms and the U_{ij} values reveal a relatively strong but positive definite anisotropy with $U_{11} \ll U_{22} \approx U_{33}$. However, this anisotropy was not sufficient to introduce a split position in the refinement. An attempt to refine mixed Al/Ir occupancy for the Al25 and Al28 position resulted in a scattering power of $Al_{0.99}Ir_{0.01}$, i.e., negligible iridium contribution, but did not influence the anisotropy level of U_{ij}. Thus for both positions we assume exclusively aluminum occupancy. The reduced U_{eq} values for these sites originate from displacement anisotropy, i.e., from the local disorder, and not from mixed Ir/Al occupancy. As may be expected in such cases, a refinement of the structure in the non-centrosymmetric space group $Pn2_1a$ neither lowered the residuals significantly ($R(F) = 0.033$ for 522 parameters and 9640 independent reflections), nor reduced the displacement anisotropy of the sites mentioned above.

Local disorder is not a rare observation in the crystal structures of intermetallic compounds. If the atom in question is located on a closed symmetry element, this leads to a breaking of the symmetry. To give some examples: in Eu_3Si_4 [19] the corrugation of the plane silicon network resulted in symmetry breaking and was correlated with the instability of the plane Si_6 groups with a tendency to locally form either chair- or boat-like conformations or with the partial replacement of the europium atoms by triangular Si_3 groups. In $Cs_8Sn_{44}\square_2$ [20], the local disorder in the tin network was caused by the partial defect in the neighboring site leading to the displacement of the remaining atoms towards the hole. In the crystal structure of $YbGa_5$ [21], the local disorder and symmetry breaking in the gallium network resulted from a tendency of three-bonded gallium atoms to form a fourth bond. Reassuming, the observations of this kind seem to be in connection with the details of the chemical bonding in the intermetallic compounds. Because of the complexity (and size) of the $Ir_{13}Al_{45}$ structure, a more detailed analysis of the chemical bonding, as was done in Refs. [19–21] is not realistic at the present (cf. also the discussion of the interatomic distances below). Nevertheless, we suggest the chemical bonding to be responsible for the unusual displacement of the Al25 and Al28 sites.

The Ir content of the single crystals was found to be 22.9(3) at% Ir by EDX analysis, which agrees well with the result of the crystal structure refinement (22.4 at% Ir). No impurities of elements heavier than Na were found in the EDX spectra.

The interatomic distances Ir–Al in $Ir_{13}Al_{45}$ can be grouped in three ranges. The first range contains distances shorter than 2.57 Å and can be interpreted in terms of the covalent radii ($r^c_{Al} = 1.25$ Å, $r^c_{Ir} = 1.26$ Å, $r^c_{sum} = 2.51$ Å [22]). The second range contains distances between 2.73Å and 2.98 Å. These can be understood by comparing them with the sum of atomic radii ($r^a_{Al} = 1.43$Å, $r^a_{Ir} = 1.36$Å, $r^a_{sum} = 2.79$Å [22]). To the third group belong the intermediate distances of

Table 3
Anisotropic atomic displacement parameters for $Ir_{13}Al_{45}$[a]

Atom	U_{11}	U_{22}	U_{33}	U_{12}	U_{13}	U_{23}
Ir1	0.0045(1)	0.0054(1)	0.0041(1)	0.0003(1)	0.0003(1)	–0.0006(1)
Ir2	0.0042(1)	0.0055(1)	0.0050(1)	–0.0009(1)	0.0002(1)	–0.0008(1)
Ir3	0.0041(1)	0.0051(1)	0.0043(1)	0.0001(1)	0.0001(1)	0.0005(1)
Ir4	0.0051(1)	0.0046(1)	0.0044(1)	0.0002(1)	0.0007(1)	0.0002(1)
Ir5	0.0064(2)	0.0045(2)	0.0064(2)	0	0.0019(2)	0
Ir6	0.0060(2)	0.0053(2)	0.0049(2)	0	–0.0007(2)	0
Ir7	0.0048(2)	0.0042(2)	0.0041(2)	0	–0.0002(2)	0
Ir8	0.0047(2)	0.0050(2)	0.0051(2)	0	–0.0007(2)	0
Ir9	0.0046(2)	0.0047(2)	0.0044(2)	0	0.0001(2)	0
Al1	0.010(1)	0.005(1)	0.009(1)	–0.002(1)	0.001(1)	0.003(1)
Al2	0.011(1)	0.007(1)	0.009(1)	–0.002(1)	–0.002(1)	0.000(1)
Al3	0.017(1)	0.006(1)	0.011(1)	–0.004(1)	0.007(1)	–0.001(1)
Al4	0.014(1)	0.007(1)	0.009(1)	0.001(1)	–0.006(1)	0.001(1)
Al5	0.013(1)	0.013(1)	0.015(1)	–0.007(1)	0.009(1)	–0.009(1)
Al6	0.012(1)	0.022(2)	0.009(1)	–0.011(1)	0.004(1)	–0.006(1)
Al7	0.009(1)	0.009(1)	0.009(1)	0.000(1)	–0.001(1)	–0.001(1)
Al8	0.011(1)	0.007(1)	0.011(1)	–0.002(1)	–0.001(1)	–0.002(1)
Al9	0.008(1)	0.012(1)	0.028(2)	0.002(1)	0.001(1)	0.010(1)
Al10	0.009(1)	0.007(1)	0.006(1)	0.001(1)	–0.001(1)	0.000(1)
Al11	0.007(1)	0.005(1)	0.009(1)	0.001(1)	0.001(1)	0.000(1)
Al12	0.022(2)	0.007(1)	0.009(1)	–0.003(1)	0.006(1)	–0.002(1)
Al13	0.005(1)	0.006(1)	0.005(1)	–0.002(1)	0.0018(9)	–0.003(1)
Al14	0.006(1)	0.009(1)	0.009(1)	0.002(1)	0.000(1)	0.000(1)
Al15	0.007(1)	0.007(1)	0.009(1)	0.001(1)	–0.001(1)	0.002(1)
Al16	0.011(1)	0.009(1)	0.008(1)	–0.002(1)	0.001(1)	0.002(1)
Al17	0.006(2)	0.007(2)	0.009(2)	0	0.002(1)	0
Al18	0.007(2)	0.007(2)	0.008(2)	0	–0.003(1)	0
Al20	0.011(2)	0.011(2)	0.006(2)	0	0.000(1)	0
Al21	0.010(2)	0.014(2)	0.003(2)	0	0.002(1)	0
Al22	0.007(2)	0.007(2)	0.010(2)	0	0.002(1)	0
Al23	0.010(2)	0.003(2)	0.004(2)	0	0.001(1)	0
Al24	0.008(2)	0.005(2)	0.007(2)	0	0.000(1)	0
Al26	0.005(2)	0.014(2)	0.009(2)	0	0.000(1)	0
Al27	0.008(2)	0.026(3)	0.015(2)	0	–0.002(2)	0
Al28	0.003(2)	0.006(2)	0.005(2)	0	0.004(1)	0
Al29	0.010(2)	0.007(2)	0.008(2)	0	0.002(1)	0

[a]The total displacement factor is calculated as $\exp\left[-2\pi^2\left(U_{11}h^2a^{*2}+U_{22}k^2b^{*2}+U_{33}l^2c^{*2}+U_{12}hka^*b^*+U_{13}hla^*c^*+U_{23}klb^*c^*\right)\right]$.

2.57–2.70 Å. Taking into account the chemical bonding investigated with the electron localization function in the chemically related compound $IrGa_2$ [23], we assume that the distances in the first range predominantly represent two-center bonds. The distances from the third range represent mainly two- and three-center bonds. Finally, the distances in the second range reflect mostly three- and multi-center bonding between Ir and Al ligands. It is impossible to give a more precise definition of the borders between the groups of bonding distances without a detailed bonding analysis. This is not realistic at present due to the large size of the unit cell.

The above-described distribution of bond lengths in the structure of $Ir_{13}Al_{45}$ results in very irregularly shaped coordination polyhedra around the Ir atoms (Fig. 2), that all are exclusively coordinated by Al. A part of the Ir atoms (Ir1, Ir4) have an environment similar to the Ir–Al system neighboring compound $IrAl_3$. Another part (Ir7) is coordinated by aluminum atoms forming a double-capped tetragonal antiprism, that resembles the next aluminum-rich structure Ir_2Al_9 [2]. Although the polyhedra lack easily recognizable symmetry elements, the assemblage of the Ir atoms on their own shows a pseudopentagonal local symmetry when seen along [100]. This regularity is also reflected in the pseudopentagonal symmetry of the $0\,k\,l$ diffraction pattern. Such arrangement of the Ir atoms lends itself well as starting point for the description of the crystal structure of $Ir_{13}Al_{45}$.

By sharing apexes, edges and triangular faces, the coordination polyhedra around the Ir atoms build up pseudopentagonal columns parallel with the *a* axis. The core of the column is formed from Ir7 and Ir9 (Fig. 3, left). This core is surrounded by polyhedra centered by Ir1–Ir5 and Ir8, building up a pseudopentagonal column (Fig. 3, middle). The columns are arranged in the

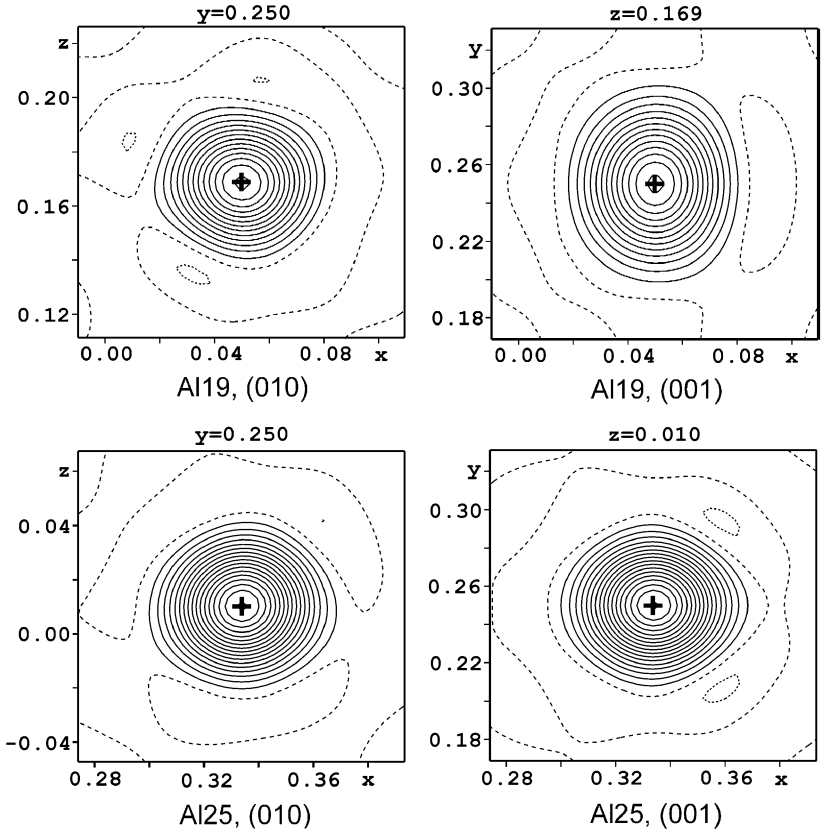

Fig. 1. Difference Fourier maps in the vicinity of the Al19 and Al25 positions calculated after the relevant atom had been removed. The cross indicates the refined position. In the case of Al19 it shows the position before splitting. The isolines are shown with the step $3\,e^{-}/Å^{3}$. Isolines representing negative values are dashed.

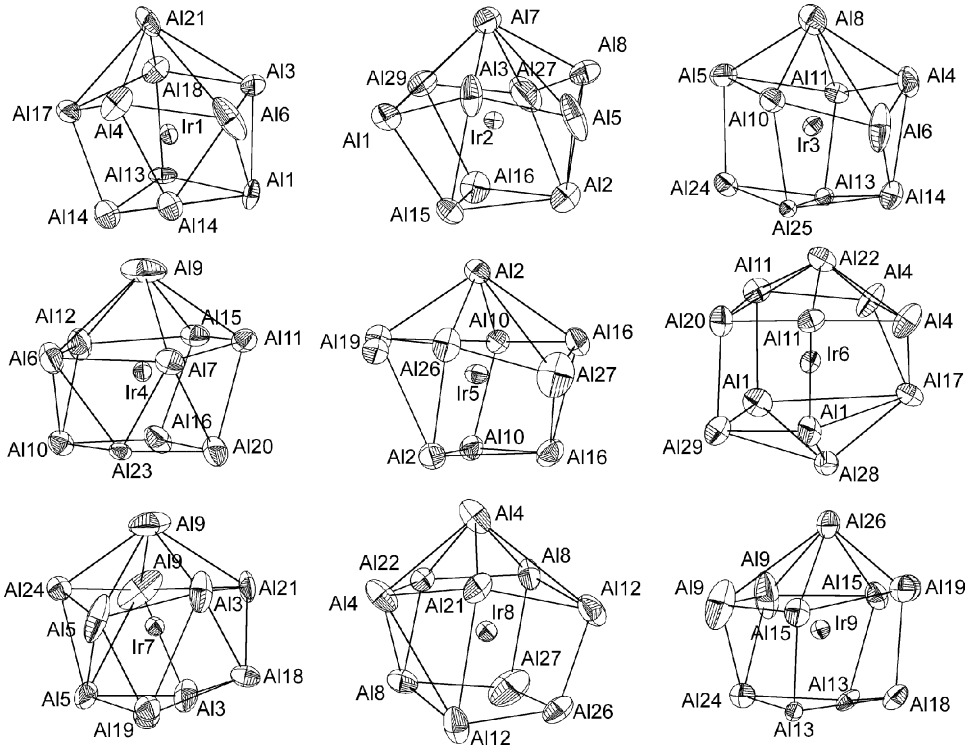

Fig. 2. Coordination polyhedra of the Ir atoms in the crystal structure of $Ir_{13}Al_{45}$. The anisotropic ellipsoids are drawn at 99.5% probability.

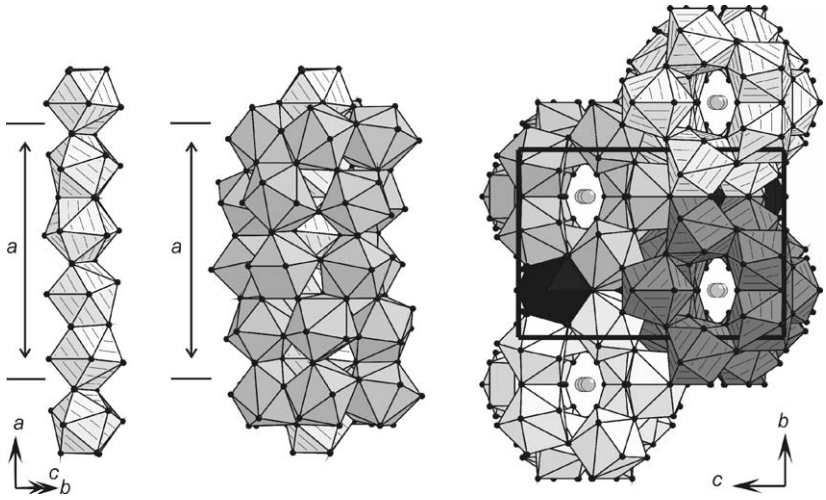

Fig. 3. The $Ir_{13}Al_{45}$ structure interpreted in terms of Ir coordination polyhedra. Iridium atoms are represented by gray spheres, aluminum atoms by black spheres. (Left) Inner rod formed by polyhedra around Ir7 and Ir9. (Middle) Pseudopentagonal environment of the inner rod, formation of the pseudopentagonal column. (Right) hexagonal arrangement of pseudopentagonal columns. Polyhedra belonging to columns at $z \approx 0.25$ are hatched and those belonging to columns at $z \approx 0.75$ are drawn in plain gray levels. Polyhedra around Ir6 are drawn in black fill the free space. For clarity, the innermost column is not drawn.

structure as a simple hexagonal column packing with the axial direction parallel with [100] (Fig. 3, right). The polyhedra belonging to two adjacent columns share both edges and triangular faces. The columns at $z \approx 0.25$ are shifted by roughly a half of the height of an Ir coordination polyhedra relative to those at $z \approx 0.75$, due to the center of symmetry located in between. Hence the columns "interlock" in a zigzag manner.

The structure of $Ir_{13}Al_{45}$ is rather dissimilar from the structures of the chemically related cobalt aluminides of Al-rich compositions. Neither in orthorhombic Co_4Al_{13} [24], nor in monoclinic Co_4Al_{13} [25], the pseudopentagonal columns of polyhedra centered by transition metal atoms form a simple hexagonal column packing. Furthermore, except for the pseudopentagonality, the columns themselves are not very similar. In Co_4Al_{13}, the polyhedra belonging to adjacent columns share square faces, leading to shorter distances between transition metal atoms than in $Ir_{13}Al_{45}$. In the Rh–Al system the monoclinic phase Rh_4Al_{13} has been reported with a structure similar to that of monoclinic Co_4Al_{13}, but without any refinement [26]. No other Al-rich binary cobalt group compound has shown such a high degree of structural complexity as $Ir_{13}Al_{45}$ reported in the present study.

The lattice parameters of the $Ir_{13}Al_{45}$ phase in the two-phase regions were found to be equal to the lattice parameters of the single-phase material within two e.s.d.'s: $a = 16.766(2)$ Å, $b = 12.318(1)$ Å, $c = 17.421(2)$ Å for $Ir_{13}Al_{45}$ in equilibrium with 'Ir_4Al_{13}' and $a = 16.760(1)$ Å, $b = 12.320(1)$ Å, $c = 17.423(1)$ Å for $Ir_{13}Al_{45}$ in equilibrium with Ir_2Al_9. Thus, the $Ir_{13}Al_{45}$ phase is formed with a constant composition.

According to the available phase diagram [9], Ir_2Al_9 decomposes on heating peritectically at 900 °C, forming a melt and 'Ir_4Al_{13}' which itself undergoes a peritectic decomposition at 1015 °C. The phase $Ir_{13}Al_{45}$ is not present in the phase diagram. Fig 4 (left) depicts the obtained DTA curve on heating in the relevant temperature range obtained from a sample containing $Ir_{13}Al_{45}$ with some admixture of Ir_2Al_9. The endothermal signal at $T_{onset} = 895$ °C (peritectic temperature of $Ir_{13}Al_{45}$) has a shoulder at lower temperatures indicating a peritectic decomposition of Ir_2Al_9 at $T_{onset} = 876$ °C. The sample with phase pure $Ir_{13}Al_{45}$ did not show this shoulder and a sample with phase pure Ir_2Al_9 showed the same onset temperature as that of the shoulder. At higher temperature the peritectic decomposition of 'Ir_4Al_{13}' at $T_{onset} = 1015$ °C is observed. This value is in full agreement with the previously reported diagram. According to [9], Ir_2Al_9 should form upon cooling from the melt with iridium concentration lower than 2.0 at%. Since crystals of $Ir_{13}Al_{45}$ formed at 1.3 at% Ir, we conclude that the liquidus at the peritectic temperature of Ir_2Al_9 should be at an iridium concentration lower than this value. Further, the kinetics of the peritectic reaction $Ir_{13}Al_{45} + \text{melt} \rightarrow Ir_2Al_9$ is evidently rather slow, since the crystals of $Ir_{13}Al_{45}$ had not yet dissolved after the slow cooling to a temperature that was 200 °C lower than the peritectic decomposition temperature of Ir_2Al_9. The observations above allow us to propose a revised phase diagram of the binary system Ir–Al in the vicinity of $Ir_{13}Al_{45}$ (Fig. 4, right). Compared with Ref. [9], the new phase $Ir_{13}Al_{45}$ has been included, the peritectic temperature of Ir_2Al_9 has been adjusted to a lower temperature and, finally, the liquidus line has been

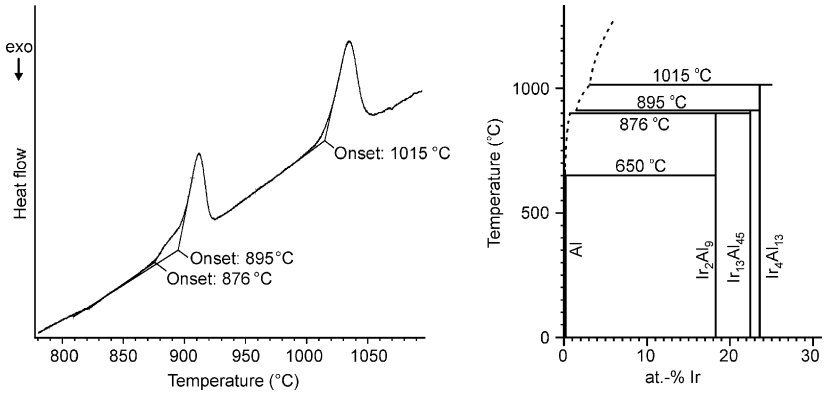

Fig. 4. (Left) DTA results (heating rate 10 K/min) on the mixture of $Ir_{13}Al_{45}$ with a small amount of Ir_2A_9. (Right) Revised aluminum-rich part of the Ir–Al binary system.

adjusted to lower iridium concentrations in the vicinity of the peritectic temperature of Ir_2Al_9.

4. Conclusions

The new binary compound $Ir_{13}Al_{45}$ is the first representative of a new structure type. The structure shows a partial local disorder in vicinity of some aluminum positions. Due to complex interactions between Ir and Al, the environments of the iridium atoms are very irregular. The complex crystal structure can be well described as a column packing of pseudopentagonal columns formed from aluminum polyhedra centered by iridium atoms. The phase $Ir_{13}Al_{45}$ forms peritectically from the melt and 'Ir_4Al_{13}' at 895 °C.

Acknowledgments

Ms. K. Schulze is thanked for the EDX analysis.

References

[1] A.M.B. Douglas, Acta Crystallogr. 3 (1950) 19–24.
[2] M. Boström, H. Rosner, Y. Prots, U. Burkhardt, Y. Grin, Z. Anorg. Allg. Chemie (2004), in press.
[3] L.E. Edshammar, Acta Chem. Scand. 21 (1967) 1104–1105.
[4] R. Ferro, R. Capelli, R. Marazza, S. Delfino, A. Borsese, G.B. Bonino, Atti Accad. Naz. Linz. 45 (1968) 556–563.
[5] K. Gotzman, U. Burkhardt, M. Ellner, Y. Grin, Powder Diffr. 12 (1997) 248–251.
[6] Y. Grin, K. Peters, U. Burkhardt, K. Gotzmann, M. Ellner, Z. Kristallogr. 212 (1997) 439–444.
[7] P. Esslinger, K. Schubert, Z. Metallkd. 48 (1957) 126–134.
[8] H. Schulz, K. Ritapal, W. Bronger, W. Klemm, Z. Anorg. Allg. Chem. 358 (1968) 299–313.
[9] K.M. Axler, E.M. Foltyn, D.E. Peterson, W.B. Hutchinson, J. Less-Common Met. 156 (1989) 213–219.
[10] L. Ma, R. Wang, K.H. Kuo, Scr. Met. 22 (1988) 1791–1796.
[11] R. Wang, L. Ma, K.H. Kuo, J. Less-Common Met. 163 (1990) 27–35.
[12] Y. Yamabe-Mitarai, Y. Ro, T. Maruko, H. Harada, Met. Trans. A. 29A (1998) 537–549.
[13] P.J. Hill, L.A. Cornish, M.J. Witcomb, J. Alloys Compd. 280 (1998) 240–250.
[14] Y. Yamabe-Mitarai, H. Aoki, P. Hill, H. Harada, Scr. Mater. 48 (2003) 565–570.
[15] M. Boström, S. Hovmöller, J. Alloys Compd. 314 (2001) 154–159.
[16] G.M. Sheldrick, SHELXS97—A Program for Automatic Solution of Crystal Structures, University of Göttingen, Germany, 1997.
[17] V. Petricek, M. Dusek, The Crystallographic Computing System, Institute of Physics, Praha, Czech Republic, 2000.
[18] J. Laugier, B. Bochu, CELREF, Laboratoire des Materiaux et du Génie Physique de l'Ecole Supérieure de Physique de Grenoble, France, 2003.
[19] F. Weitzer, Yu. Prots, W. Schnelle, K. Hiebl, Yu. Grin, J. Solid State Chem. 177 (2004) 2115–2121.
[20] H.G. von Schnering, R. Kröner, M. Baitinger, K. Peters, R. Nesper, Yu. Grin, Z. Kristallogr. NCS 215 (2000) 205–206.
[21] R. Giedigkeit, R. Niewa, W. Schnelle, Yu. Grin, R. Kniep, Z. Anorg. Allg. Chem. 628 (2002) 1692–1696.
[22] J. Emsley, Elements, Oxford University Press, Oxford, 1997.
[23] M. Boström, Y. Prots, Yu. Grin, J. Solid State Sci. 6 (2004) 499–503.
[24] Yu. Grin, U. Burkhardt, M. Ellner, K. Peters, J. Alloys Compd. 206 (1994) 243–247.
[25] R.C. Hudd, W.H. Taylor, Acta Crystallogr. 15 (1962) 441–442.
[26] Z.A. Chaudhury, C. Suryanarayana, J. Less-Common Met. 91 (1983) 181–187.
[27] P.J. Becker, P. Coppens, Acta Crystallogr. A 30 (1974) 129–153.